Cross sections for elastic electron–hydrogen sulfide collisions in the low- and intermediate-energy range

P. Rawat, I. Iga, and M.-T. Lee
Departamento de Química, Universidade Federal de São Carlos, 13565-905 São Carlos SP, Brazil

L. M. Brescansin
Instituto de Física "Gleb Wataghin," UNICAMP, 13083-970 Campinas SP, Brazil

M. G. P. Homem and L. E. Machado
Departamento de Física, Universidade Federal de São Carlos, 13565-905 São Carlos SP, Brazil
(Received 8 January 2003; published 14 November 2003)

In this work, we present a joint theoretical and experimental study on electron-H_2S collisions in the low- and intermediate-energy range. More specifically, we report measured elastic differential, integral, and momentum-transfer cross sections in the (100–500)-eV energy range. In addition, calculated elastic cross sections in the (0.5–500)-eV energy range are also reported. The measurements were performed using a crossed electron beam–molecular beam geometry. The angular distributions of the scattered electrons were converted to absolute cross sections using the relative flow technique. Theoretically, an optical potential is used to represent the electron-molecule interaction. The Schwinger variational method combined with the distorted-wave approximation is used to solve the scattering equations. The comparison between our calculated and measured results as well as with other available experimental and theoretical data in the literature is encouraging.

DOI: 10.1103/PhysRevA.68.052711 PACS number(s): 34.80.Bm

I. INTRODUCTION

Electron-polar molecule scattering cross sections are of fundamental importance in a great variety of physical and chemical processes and thus their determination has been a subject of continuously increasing experimental and theoretical interest [1]. Particularly, hydrogen sulfide (H_2S) is an interesting molecule and has attracted attention due to its participation in a great number of processes. For example, the presence of H_2S was found [2] in the comet Austin (1989C1) as well as in interstellar molecular clouds [3]. Also, H_2S is known as one of the major pollutants of Earth's atmosphere which gives origin to corrosive processes in metals [4]. So e^--H_2S collisions may be important for some astrophysical and environmental applications. Moreover, an atmosphere of H_2S is used [5] in the synthesis of a semiconductor, tungsten disulfide (WS_2), whose molecular structure is identical to fullerene (C_{60}). Also, a mixture of N_2, H_2, and H_2S is used in plasma nitrocarburizing processes [6]. Since H_2S is a strongly polar molecule, its presence in a gas, even as a minor impurity, can affect significantly its physical properties, such as the electrical conductivity.

Despite its importance, only recently has low-energy electron scattering by hydrogen sulfide been more extensively studied. During the past two decades, most experimental investigations on electron-H_2S collisions were performed for incident energies below 30 eV. For this energy range, total (elastic+inelastic) cross sections (TCS's) were first measured by Sokolov and Sokolova [7] and then by Szmytkowski and Maciąg [8]. About ten years ago, Gulley *et al.* [3] reported measured vibrationally elastic and inelastic differential cross sections (DCS's) in the angular range of 10°–130° for incident energies up to 30 eV. On the theoretical side, earlier studies on e^--H_2S scattering include calculations of elastic and vibrational excitation cross sections [9], elastic, rotational excitation, and vibrational excitation DCS's, integral cross sections (ICS's) and momentum-transfer cross sections (MTCS's) [10], and elastic (rotationally summed) [11,12] and rotationally inelastic cross sections [11]. These calculations have in common the use of an *ab initio* static and a model exchange plus polarization potential (SEP). Rotationally and vibrationally unresolved elastic e^--H_2S scattering cross sections were calculated by Machado *et al.* [13] using an exact static-exchange (SE) potential plus Born-closure procedure to account for high partial-wave contributions. Very recently, low-energy elastic e^--H_2S scattering was studied by Varella *et al.* [14] using the Schwinger multichannel method (SMC) with pseudopotentials at the SE level, combined with a Born-closure procedure.

Above 30 eV, both theoretical and experimental studies are scarce. Total cross sections have been measured by Zecca *et al.* [15] in the (75–4000)-eV energy range. Total ionization cross sections have been measured by Rao and Srivasatava [16] at incident energies up to 1000 eV. Theoretically, ICS's as well as TCS's were reported by Jain and Baluja [17], using a spherical complex optical potential (SCOP) in the (50–5000)-eV energy range. Also, total cross sections were calculated by Joshipura *et al.* [18] and by Jiang *et al.* [19], both using the additivity rule and a complex atomic potential composed of SEP plus absorption contributions. To our knowledge, the only article reporting DCS's for $E_0 \geqslant 50$ eV is that of Jain *et al.* [20], who also employed an SCOP model. However, no measured elastic DCS's in this energy range have ever been reported in the literature.

Considering the importance of this molecule in various areas of application, the knowledge of reliable experimental

cross sections for electron-H_2S scattering in the intermediate energy range (50–500 eV) will certainly be very interesting, not only for practical applications but also for stimulating the development of new theoretical and computational methods that can provide important data for comparison. A reliable theoretical study of the e^--H_2S elastic scattering requires accurate descriptions for both short- and long-range interaction potentials. A fixed-nuclei treatment of electron scattering by polar molecules is known to lead to divergent elastic DCS's in the forward direction, due to the slow falloff of the partial-wave *T*-matrix elements for large *l* [21]. This divergence can be removed only by the introduction of nuclear motion in the Hamiltonian [22]. It is well known that absorption effects play an important role in electron-molecule scattering in the intermediate energy range (from ionization threshold to a few hundreds eV). Although the main features of these effects are known, taking them into account in an *ab initio* treatment of electron-molecule scattering is a very difficult task. Therefore, the use of model absorption potentials seems to be presently the only practical manner for such a purpose.

In this paper, we perform a joint theoretical and experimental study for electron scattering by H_2S in the low- and intermediate-energy range. The purpose of the present work is twofold: (i) to provide experimental values of cross sections for elastic e^--H_2S scattering for energies $E_0 \geqslant 100$ eV, and (ii) to use these cross sections as a check of our theoretical method. In particular, we report measured DCS's, ICS's, and MTCS's from 100 to 500 eV. Calculated DCS's as well as ICS's and MTCS's for incident energies ranging from 0.5 to 500 eV are also reported and compared with the present and other experimental and/or theoretical results available in the literature.

Our experimental absolute elastic DCS's are determined using the relative flow technique (RFT) [23–31]. Theoretically, a complex optical potential which includes static, exchange, correlation-polarization, and absorption contributions is used to represent the interaction dynamics, while a combination of the Schwinger variational iterative method (SVIM) [32] and the distorted-wave approximation (DWA) [33–35] is used to calculate accurate *ab initio* low-*l* partial-wave scattering. Rotationally elastic and inelastic cross sections are calculated separately within the framework of the adiabatic-nuclei-rotation (ANR) approximation. Higher angular-momentum dipole-potential components are then added to infinity through a first Born approximation (FBA) closure formula. Rotationally unresolved cross sections are obtained by summing up the rotationally elastic and inelastic contributions.

The organization of this paper is as follows. In Sec. II, we describe briefly the theory used and also give some details of the calculation. In Sec. III, some experimental details are briefly described. Finally, in Sec. IV, we compare our calculated results with the present experimental and other existing theoretical and experimental data.

II. THEORY AND CALCULATION

In this section, we will briefly discuss the method used; details of the SVIM and the DWA can be found elsewhere [32–35]. Within the ANR framework, the DCS for the excitation of an asymmetric-top rotor from an initial rotational level $J\tau$ to a final level $J'\tau'$ is given by

$$\frac{d\sigma}{d\Omega}(J\tau \to J'\tau') = \frac{1}{2\pi}\frac{1}{(2J+1)}\frac{k_{J'\tau'}}{k_{J\tau}} \times \sum_{M=-J}^{J}\sum_{M'=-J'}^{J'}\int_0^{2\pi} d\phi \ |f_{J\tau M\to J'\tau' M'}|^2, \tag{1}$$

where $f_{J\tau M\to J'\tau' M'}$ is the rotational excitation scattering amplitude related to the rotational eigenfunctions of the target by

$$f_{J\tau M\to J'\tau' M'} = \langle \Psi_{J'\tau' M'}(\Omega)|f^{\mathrm{LF}}|\Psi_{J\tau M}(\Omega)\rangle, \tag{2}$$

$k_{J\tau}$ and $k_{J'\tau'}$ are the magnitudes of the linear momenta of the incident and the scattered electron, respectively, and $\Omega \equiv (\alpha,\beta,\gamma)$ are the Euler angles defining the frame transformation [36]. The eigenfunctions $\Psi_{J\tau M}(\Omega)$ appearing in Eq. (2) are written as linear combinations of symmetric-top eigenfunctions [37],

$$\Psi_{J\tau M}(\Omega) = \sum_{K=-J}^{J} a_{KM}^{J\tau}\Phi_{JKM}(\Omega), \tag{3}$$

where the symmetric-top eigenfunctions are given by

$$\Phi_{JKM}(\Omega) = \left(\frac{2J+1}{8\pi^2}\right) D_{KM}^{J*}(\Omega), \tag{4}$$

where D_{KM}^{J} are the well-known Wigner rotation matrices [37]. Also, f^{LF} appearing in Eq. (2) is the electronic part of the laboratory-frame (LF) scattering amplitude which can be related to the corresponding body-frame (BF) *T* matrix by a usual frame transformation. The latter can be conveniently partial-wave expanded as

$$T = \frac{1}{k}\sum_{p\mu lhl'h'} i^{l-l'} T^{p\mu}_{k,lh;l'h'} X^{p\mu}_{lh}(\hat{k}) X^{p\mu *}_{l'h'}(\hat{k}_0), \tag{5}$$

where $\hat{k}_0$ and $\hat{k}$ are the linear momentum directions of the incident and scattered electrons in BF, respectively, and $X^{p\mu}_{lh}(\hat{k})$ are the symmetry-adapted functions [38] which are expanded in terms of the usual spherical harmonics as follows:

$$X^{p\mu}_{lh}(\hat{r}) = \sum_m b^{p\mu}_{lhm} Y_{lm}(\hat{r}). \tag{6}$$

Here *p* is an irreducible representation (IR) of the molecular point group, μ is a component of this representation, and *h* distinguishes between different bases of the same IR corresponding to the same value of *l*. The coefficients $b^{p\mu}_{lhm}$ satisfy important orthogonality relations and are tabulated for C_{2v} and O_h point groups [38].

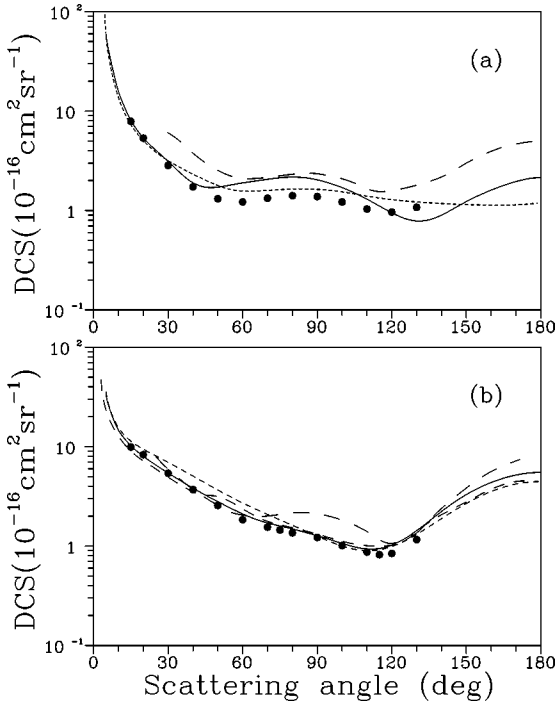

FIG. 1. DCS's for elastic e^--H_2S scattering at the impact energy of (a) 2 eV and (b) 5 eV. Solid line, present rotationally summed results; dotted line, SVIM results of Machado *et al.* [13]; short-dashed line, SMC results of Varella *et al.* [14]; dashed line, results of Nishimura *et al.* [9]; long-dashed line, theoretical results of Greer and Thompson [12]; full circles, experimental results of Gulley *et al.* [3].

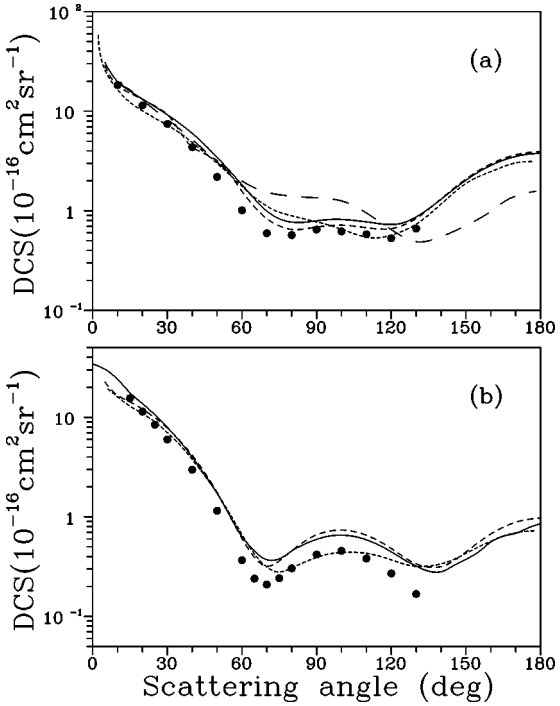

FIG. 2. Same as Fig. 1 but for (a) 10 and (b) 20 eV. The symbols are the same as in Fig. 1, except long-dashed line, theoretical results of Gianturco [11].

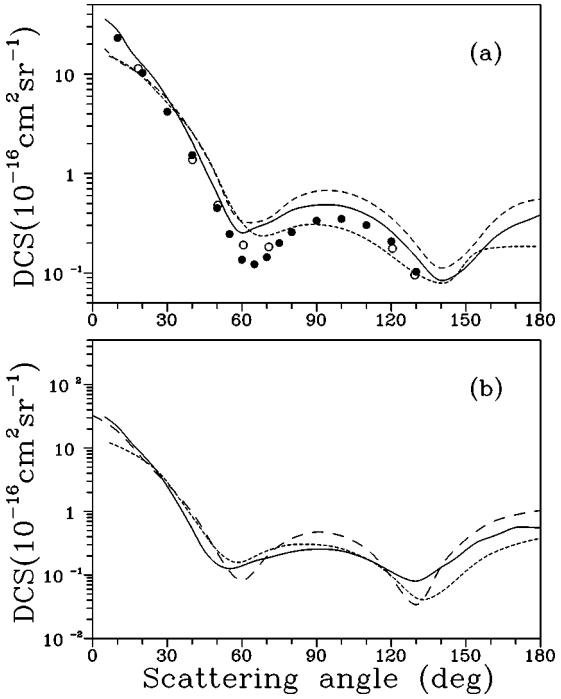

FIG. 3. Same as Fig. 2 but for (a) 30 and (b) 50 eV. The symbols are the same as in Fig. 2, except dashed line, theoretical results of Jain *et al.* [20]; open circles: experimental data of Marinkovič [49].

In the present study, the electron-molecule scattering dynamics is represented by an interaction potential given by

$$V(\vec{r}) = V_{\mathrm{SEP}} + iV_{\mathrm{ab}}, \tag{7}$$

where V_{SEP} is the sum of the static (V_{st}), the exchange (V_{ex}), and the correlation-polarization (V_{cp}) contributions, and V_{ab} is the absorption potential. In our calculation, V_{st} and V_{ex} are derived exactly from a Hartree-Fock self-consistent-field (SCF) target wave function. The electronic configuration of the ground-state H_2S is $1a_1^2 2a_1^2 3a_1^2 1b_1^2 1b_2^2 4a_1^2 2b_2^2 5a_1^2 2b_1^2$, X^1A_1. The SCF wave function is calculated from standard contracted basis sets of Huzinaga [39] augmented by one s ($\alpha = 0.0335$), three p ($\alpha = 1.120$, 0.271, and 0.0697) uncontracted functions on the hydrogen centers and three s ($\alpha = 0.0507$, 0.0171, and 0.0057), four p ($\alpha = 0.0503$, 0.0167, 0.0053, and 0.0027), and two d ($\alpha = 1.4137$ and 0.3043) uncontracted functions on the sulfur center. At the experimental equilibrium geometry ($R_{\mathrm{H\text{-}S}} = 2.52$ a_0 and $\theta_{\mathrm{H\text{-}S\text{-}H}} = 92.2°$), this basis set gives an SCF energy of -398.68 a.u. which compares well with the calculated value of -398.61 a.u. [40] and an electric dipole moment of 0.43 a.u., exactly the same calculated value of Greer and Thompson [12]. The experimental dipole moment is 0.38 a.u. [11].

A parameter-free model potential introduced by Padial and Norcross [41] is used to account for the correlation-polarization contributions. In this model, a short-range correlation potential between the scattering and the target electrons is defined in an inner interaction region and a long-range polarization potential in an outer region. The

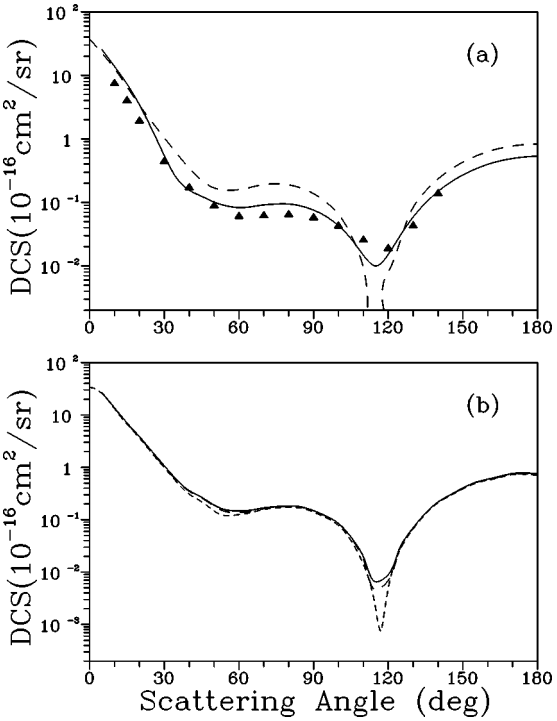

FIG. 4. (a) Same as Fig. 3 but for 100 eV. The symbols are the same as in Fig. 3, except triangles, present experimental results; (b) rotationally resolved DCS's for the $(J=0\rightarrow J'=0)$ transition (short-dashed line); rotationally summed DCS's up to $J'=1$ (dashed line) and $J'=2$ (solid line).

correlation potential is calculated by a free-electron-gas model, derived using the target electronic density according to Eq. (9) of Padial and Norcross [41]. In addition, an asymptotic form of the polarization potential is used for the

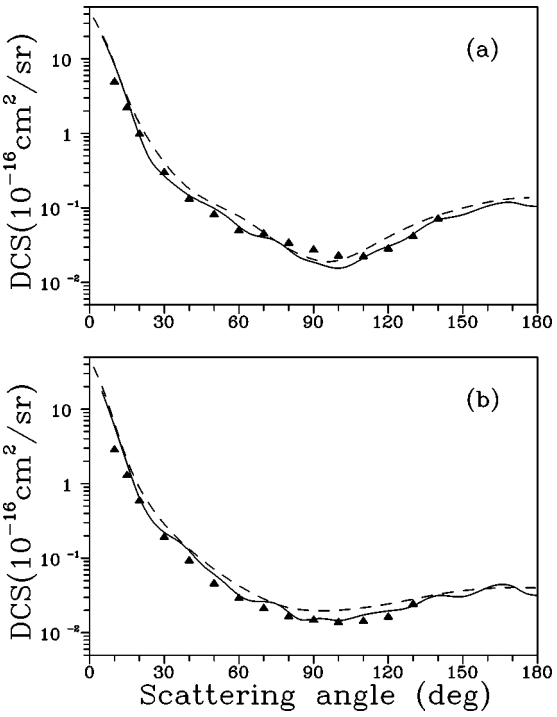

FIG. 5. Same as Fig. 4(a) but for (a) 300 and (b) 500 eV.

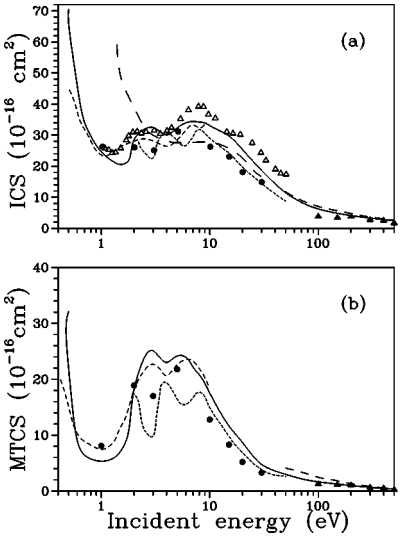

FIG. 6. (a) ICS's and (b) MTCS's for elastic e^--H_2S scattering. Solid line, present rotationally summed results; dotted line, SVIM results of Machado *et al.* [13]; short-dashed line, theoretical results of Jain and Thompson [10]; dashed line, results of Jain *et al.* [20]; long-dashed line, theoretical results of Gianturco [11]; full circles, experimental results of Gulley *et al.* [3]; open triangles, experimental TCS's of Szmytkowski and Maciąg [8]; full triangles, present experimental results.

long-range electron-target interaction. Only the spherical part of $V_{\rm cp}$ was used in our calculations and the dipole polarizability $\alpha_0=24.55$ a.u. [42] was used to calculate the asymptotic form of $V_{\rm cp}$. The first crossing of the correlation and polarization potential curves defines the inner and the outer region. No cutoff or other adjusted parameters are needed for the calculation of $V_{\rm cp}$.

The absorption potential $V_{\rm ab}$ in Eq. (7) is given as

$$V_{\rm ab}(\vec{r})=-\rho(\vec{r})\left(\frac{T_L}{2}\right)^{1/2}\left(\frac{8\pi}{5k^2k_F^3}\right)H(\alpha+\beta-k_F^2)(A+B+C), \tag{8}$$

where

$$T_L=k^2-V_{\rm SEP}, \tag{9}$$

$$A=\frac{5k_F^3}{(\alpha-k_F^2)}, \tag{10}$$

$$B=-\frac{k_F^3[5(k^2-\beta)+2k_F^2]}{(k^2-\beta)^2}, \tag{11}$$

and

$$C=2H(\alpha+\beta-k^2)\frac{(\alpha+\beta-k^2)^{5/2}}{(k^2-\beta)^2}. \tag{12}$$

In Eqs. (8)–(12), k^2 is the energy (in Rydbergs) of the incident electron, k_F the Fermi momentum, and $\rho(\vec{r})$ the local electronic density of the target. $H(x)$ is a Heaviside function

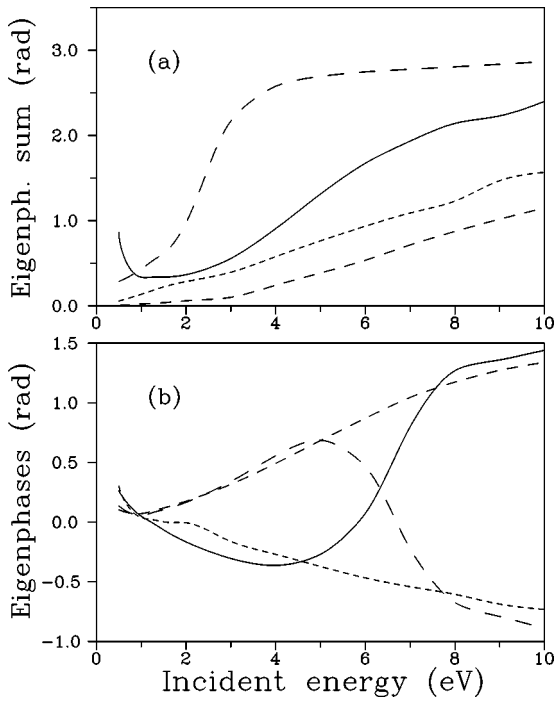

FIG. 7. (a) Eigenphase sums in the (0–10)-eV range. Solid line, $^2A_1$ symmetry; short-dashed line, $^2A_2$ symmetry; dashed line, $^2B_1$ symmetry; long-dashed line, $^2B_2$ symmetry; (b) individual eigenphases for the $^2A_1$ symmetry. Solid line, δ_{00} component; short-dashed line, δ_{10} component; dashed line, δ_{20} component; long-dashed line, δ_{22} component.

defined by $H(x)=1$ for $x\geqslant 0$ and $H(x)=0$ for $x<0$. According to Staszewska *et al.* [43],

$$\alpha(\vec{r},E)=k_F^2+2(2\Delta-I)-V_{\mathrm{SEP}}, \tag{13}$$

and

$$\beta(\vec{r},E)=k_F^2+2(I-\Delta)-V_{\mathrm{SEP}}, \tag{14}$$

where Δ is the average excitation energy and I is the ionization potential.

In principle, the Lippmann-Schwinger scattering equation for elastic e^--H_2S scattering with the full complex optical interaction potential can be solved using SVIM. Nevertheless, a tremendous computational effort would be required, particularly due to the large number of coupled equations involved, which makes such calculations practically prohibitive. On the other hand, our calculation has revealed that the magnitude of the imaginary part (absorption) of the optical potential is considerably smaller than its real counterpart. Therefore, in the present study, the scattering equations are solved using SVIM considering only the real part of the optical potential. The absorption part of the T matrix is calculated via the DWA in the two-potential formalism. According to this formalism, the interaction potential is split as

$$V_{\mathrm{opt}}=V_1+V_2, \tag{15}$$

TABLE I. Calculated DCS's, ICS's, and MTCS's (in 10^{-16} cm^2) for elastic e^--H_2S scattering.

Angle	E_0 (eV)					
(deg)	2	5	10	20	30	50
5	6.046	10.31	19.62	35.67	35.56	30.76
10	28.72	19.06	21.89	29.00	27.48	21.61
20	4.972	7.170	12.78	14.01	12.44	7.915
30	2.377	5.077	8.949	8.046	5.725	2.476
40	1.356	3.639	5.779	4.027	2.072	0.530
50	0.690	2.531	3.312	1.732	0.626	0.148
60	1.325	2.008	1.684	0.621	0.252	0.139
70	1.484	1.599	0.946	0.366	0.314	0.185
80	2.000	1.459	0.721	0.461	0.427	0.231
90	1.792	1.217	0.777	0.613	0.481	0.255
100	1.568	1.072	0.831	0.668	0.472	0.239
110	0.961	0.904	0.774	0.605	0.387	0.178
120	0.668	1.003	0.745	0.463	0.261	0.112
130	0.583	1.424	0.878	0.326	0.145	0.080
140	1.082	2.221	1.303	0.279	0.084	0.131
150	1.876	3.303	2.024	0.365	0.114	0.247
160	2.798	4.423	2.864	0.552	0.210	0.396
170	3.648	5.196	3.450	0.648	0.306	0.563
180	3.864	5.928	4.089	0.918	0.386	0.552
ICS's	28.47	32.33	33.05	24.78	18.62	11.44
MTCS's	18.13	24.18	17.52	7.991	4.756	2.984

where $V_1=V_{\mathrm{SEP}}$ and V_2 is the imaginary absorption potential. The corresponding distorted wave functions satisfy the following scattering equation:

$$(H_0+V_1-E)\chi=0, \tag{16}$$

which is solved using SVIM. Thus, the T matrix is also split into two components,

$$T=T_{\mathrm{SEP}}+T_{\mathrm{abs}}, \tag{17}$$

where T_{abs} is calculated via the DWA as

$$T_{\mathrm{abs}}=i\langle\chi_f^-|V_{ab}|\chi_i^+\rangle, \tag{18}$$

and the superscripts $(+)$ and $(-)$ denote the incoming-wave and outgoing-wave boundary conditions, respectively.

In SVIM calculations, the continuum wave functions are single-center expanded as

$$\chi_{\vec{k}}^{\pm}(\vec{r})=\left[\frac{2}{\pi}\right]^{1/2}\sum_{lm}\frac{(i)^l}{k}\chi_{klm}^{\pm}(\vec{r})Y_{lm}(\hat{k}). \tag{19}$$

In the present study, we have limited the partial-wave expansion of the continuum wave functions as well as of the T-matrix elements up to $l_c=22$ and $h_c=22$. Since H_2S is a polar molecule, these partial-wave expansions converge slowly due to the long-range dipole interaction potential. Therefore, a Born-closure formula is used to account for the contribution of higher partial-wave components to the scattering amplitudes. Accordingly, Eq. (5) is rewritten as

$$T = T^B + \frac{1}{k} \sum_{p\mu lhl'h'}^{LL'} i^{l-l'} (T^{p\mu\,\mathrm{SVIM}}_{k,lh;l'h'} - T^{p\mu\,B}_{k,lh;l'h'}) \times X^{p\mu}_{lh}(\hat{k}) X^{p\mu\,*}_{l'h'}(\hat{k}_0), \quad (20)$$

where $T^{p\mu\,\mathrm{SVIM}}_{k,lh;l'h'}$ are the partial-wave T-matrix elements calculated via SVIM and truncated to the cutoff values $L=(l_c,h_c)$ and $L'=(l'_c,h'_c)$, $T^{p\mu\,B}_{k,lh;l'h'}$ are the corresponding partial-wave point-dipole FBA T-matrix elements, and T^B is the complete point-dipole FBA T matrix, whose elements are given by

$$T^{\mathrm{Born}}_{ll'm} = -\frac{D}{l_>}\left[\frac{(l_>+m)(l_>-m)}{(2l_>+1)(2l_>-1)}\right]^{1/2}, \quad (21)$$

where $l_>=l'$ when $l'=l+1$ and $l_>=l$ when $l'=l-1$.

The rotationally unresolved DCS's for elastic e^--molecule scattering are calculated via a summation of all rotationally resolved DCS's,

$$\frac{d\sigma}{d\Omega} = \sum_{J,\tau} \frac{d\sigma}{d\Omega}(J\tau \leftarrow 00). \quad (22)$$

Sufficient rotational states were included in the above equation to ensure the convergence to be within 0.2%.

III. EXPERIMENT

Details of our experimental setup and procedure have already been presented elsewhere [44]. Basically, a crossed electron beam–molecular beam geometry is applied to measure the relative intensity of the scattered electrons as a function of the scattering angles. The electron gun used is composed of a hairpin tungsten filament, a triode extraction, a set of einzel lenses, and a set of quadrupole electrostatic deflectors which allow better positioning of the electron beam in the interaction region. The electron beam with an estimated diameter of 1 mm is generated without prior energy selection. The typical beam current is in hundreds of nA in the covered energy range. A molecular beam flows into the vacuum chamber via a capillary array. This array has a length $L=5$ mm with the individual capillary diameter $D=0.05$ mm and an aspect ratio $\gamma=D/L=0.01$. The scattered electrons are energy-filtered by a retarding-field energy selector with a resolution of about 1.5 eV. This resolution is sufficient to distinguish electronically inelastic scattered electrons. After being energy-analyzed, the elastically scattered electrons are detected by a microchannel plate.

During the measurements, the working pressure in the vacuum chamber is around 5×10^{-7} torr. The recorded scattering intensities are converted into absolute elastic DCS's using the RFT [23]. Accordingly, the DCS's for a gas x under determination can be related with the known DCS's of a secondary standard gas "std" as

$$(\mathrm{DCS})_x = (\mathrm{DCS})_{\mathrm{std}} \frac{I_x}{I_{\mathrm{std}}} \frac{n_{\mathrm{std}}}{n_x} \left(\frac{M_{\mathrm{std}}}{M_x}\right)^{1/2}, \quad (23)$$

TABLE II. Calculated DCS's, ICS's, and MTCS's (in 10^{-16} cm^2) for elastic e^--H_2S scattering.

Angle	E_0 (eV)					
(deg)	100	150	200	300	400	500
5	25.82	23.76	22.36	20.17	18.46	17.10
10	15.13	12.26	10.49	8.279	6.882	5.878
20	3.477	2.052	1.435	0.939	0.749	0.644
30	0.541	0.313	0.284	0.266	0.242	0.221
40	0.132	0.138	0.141	0.147	0.143	0.125
50	0.091	0.086	0.095	0.099	0.079	0.061
60	0.079	0.082	0.080	0.056	0.039	0.032
70	0.091	0.077	0.061	0.040	0.032	0.026
80	0.093	0.059	0.040	0.027	0.022	0.019
90	0.076	0.035	0.024	0.019	0.017	0.015
100	0.042	0.015	0.013	0.015	0.016	0.015
110	0.015	0.008	0.015	0.021	0.020	0.017
120	0.018	0.026	0.031	0.030	0.024	0.020
130	0.061	0.067	0.062	0.045	0.031	0.023
140	0.157	0.138	0.111	0.069	0.046	0.032
150	0.278	0.214	0.154	0.081	0.048	0.030
160	0.402	0.290	0.201	0.106	0.063	0.040
170	0.514	0.355	0.237	0.118	0.067	0.042
180	0.522	0.355	0.230	0.104	0.054	0.032
ICS's	6.235	4.814	4.096	3.284	2.788	2.404
MTCS's	1.641	1.241	0.982	0.664	0.483	0.371

where I is the scattered electron intensity, n is the flow rate, and M is the molecular weight. The above equation is valid if the density distributions of both gases, x and std, are close to the same. According to Olander and Kruger [45], this requirement is fulfilled under two conditions: the mean free paths λ of both gases behind the capillaries should be equal and the Knudsen number K_L, defined as λ/L, must satisfy the relation $\gamma \leqslant K_L \leqslant 10$. However, several recent investigations have provided experimental evidence that even at beam flow regimes in which the K_L's are significantly lower than γ, Eq. (20) can still be valid [29,31].

In the present study, Ar is used as the secondary standard. The collisional diameters of Ar and H_2S are 2.95 Å [46] and 3.24 Å, respectively. The latter was calculated using the van der Waals constants reported in the *Handbook of Chemistry and Physics* [47]. Thus the theoretical pressure ratio for equal K_L will be approximately 1.2:1. We used the working pressure of 5 torr for Ar and 4.14 torr for H_2S. This corresponds to $\lambda=16.1$ μm and $K_L=0.0032$. In addition, the e^--Ar absolute cross sections of Jansen *et al.* [48] in the (100–500)-eV energy range are used to normalize our data.

Details of the analysis on experimental uncertainties have also been given elsewhere [44]. They are estimated briefly as follows. Uncertainties of a random nature, such as the pressure fluctuations, electron beam current readings, background scattering, etc., are estimated to be less than 2%. These contributions combined with the estimated statistical errors give an overall uncertainty of 4% in the relative DCS's for each gas. Also, the experimental uncertainty associated with the normalization procedure is estimated to be

5.7%. These errors combined with the quoted errors [48] in the absolute DCS's of the secondary standard provide an overall experimental uncertainty of 11% in our absolute DCS's.

The absolute DCS's were determined in the 10°–140° angular range. In order to obtain ICS's and MTCS's, an extrapolation procedure was adopted to estimate DCS's at scattering angles out of that range. The extrapolation was carried out following the trend of the theoretical DCS's in both forward and backward directions. The overall errors on ICS's and MTCS's are estimated to be 22%.

IV. RESULTS AND DISCUSSION

In Figs. 1–3, we show the calculated DCS's (rotationally summed) for elastic e^--H_2S scattering in the incident energy range of 2–50 eV along with the experimental data of Gulley *et al.* [3] and Marinkovič [49], and the theoretical results of Nishimura and Itikawa [9], Gianturco [11], Greer and Thompson [12], Machado *et al.* [13], Varella *et al.* [14], and Jain *et al.* [20]. In the (2–30)-eV range, our calculated results are in good agreement both in shape and magnitude with the measured results. Also, good agreement is seen when our calculated DCS's are compared with the recent SMC results of Varella *et al.* (including contributions up to $J'=7$), with those of Nishimura and Itikawa, and those of Machado *et al.* At 50 eV, a comparison is made with the calculated SE results of Machado *et al.* and the SCOP results of Jain *et al.* Although qualitative agreement is seen among these theoretical results, there are quantitative discrepancies, especially in the forward and backward direction due to the effect of the polarization potential. Unfortunately, there are no experimental results available for comparison in the literature.

In Figs. 4 and 5, we compare our calculated DCS's (rotationally summed) with the present measured data for elastic e^--H_2S scattering in the incident energy range of 100–500 eV. The calculated results of Jain *et al.* [20] are also shown for comparison. For all energies studied herein, our calculated results agree very well with our measured data both in shape and magnitude. Particularly, the sharp increase of DCS's at small scattering angles is due to the polar nature of the target. This low-angle scattering behavior is well described by our calculation. In addition, the agreement with the theoretical results of Jain *et al.* is also very good except at 100 eV, where their results exhibit a very deep minimum at around 117°, not seen either in our calculation or in the experimental data. This discrepancy is due to the fact that only the spherical part of the interaction potential is considered in their calculation. The SCOP model of Jain *et al.* treats the H_2S molecule as its isoelectronic Ar atom. Such deep minima are very common in electron-atom scattering. For example, the DCS's for elastic e^--Ar scattering at 100 eV exhibit a deep minimum at around 117° [50,51]. Also, we have recently reported a rotationally resolved calculation for e^--H_2O scattering [52], where deep minima at around 105° are seen in the DCS's for the $(J=0\rightarrow J'=0)$ rotational transition. It is known that for this transition, only the diagonal *T*-matrix elements contribute to the DCS's. This situation is similar to the use of the SCOP model, where the *T* matrix is diagonal. However, in our calculation, the nondiagonal *T*-matrix elements contribute to other rotational transitions whose DCS's may or may not have deep minima in different angular regions. Therefore, in our rotationally unresolved DCS's these minima are smoothed out, as can be seen in Fig. 4(b), where the DCS's summed up to $J'=1$ and 2 are shown. Nevertheless, a deep minimum can be seen in our calculated rotationally resolved DCS's for the $(J=0\rightarrow J'=0)$ rotational transition at 100 eV. The results shown in Fig. 4(b) clearly come in support of the above arguments.

TABLE III. Experimental DCS's, ICS's, and MTCS's (in 10^{-16} cm^2) for elastic e^--H_2S scattering.

Angle (deg)	E_0 (eV) 100	150	200	300	400	500
10	7.724	6.924	7.421	5.069	4.830	2.943
15	4.129	3.155	3.626	2.285	1.932	1.333
20	1.983	1.503	1.516	1.012	0.843	0.610
30	0.460	0.383	0.401	0.309	0.266	0.197
40	0.177	0.177	0.175	0.136	0.124	0.095
50	0.092	0.096	0.106	0.084	0.072	0.047
60	0.063	0.073	0.085	0.051	0.041	0.030
70	0.064	0.075	0.068	0.046	0.038	0.022
80	0.067	0.056	0.047	0.035	0.036	0.017
90	0.060	0.043	0.034	0.028	0.032	0.015
100	0.044	0.028	0.025	0.024	0.029	0.014
110	0.027	0.017	0.020	0.023	0.029	0.015
120	0.020	0.021	0.034	0.029	0.033	0.017
130	0.045	0.052	0.067	0.043	0.039	0.025
140	0.142	0.135	0.126	0.074	0.057	
ICS's	4.050	3.681	4.035	2.962	2.749	1.896
MTCS's	1.415	1.281	1.184	0.769	0.656	0.376

Figures 6(a) and 6(b) show our calculated ICS's and MTCS's, respectively, in the (0.5–500)-eV energy range, along with the measured data of Gulley *et al.* [3] at energies up to 30 eV and our present experimental results in the (100–500)-eV range. The experimental TCS's of Szmytkowski and Maciąg [8] for energies from 1.3 to 50 eV are also included for comparison, since at such impact energies the elastic scattering channel dominates the electron-H_2S collisional processes. Our results are also compared with some calculated ICS's and MTCS's reported in the literature [10,11,13,20]. Quantitatively, our calculated ICS's and MTCS's show a good agreement with our measured data in the (100–500)-eV energy range. At lower energies, our calculated data agree reasonably well with the experimental results of Gulley *et al.* [3]. In addition, our ICS's also agree well with the TCS's of Szmytkowski and Maciąg [8]. Comparison with other theoretical studies has revealed a general good agreement, except with the ICS's of Gianturco [11].

It is interesting to note that both our calculated ICS's and MTCS's show some structures, namely a deep minimum located at around 1.5 eV and a shallow one at around 4 eV, the latter lying between two resonancelike features centered at around 3 eV and 7 eV. These structures were confirmed by

the experimental TCS's of Szmytkowski and Maciąg [8]. On the other hand, the experimental data of Gulley *et al.* have revealed only one minimum located at about 3 eV. Comparing with other calculations, it is seen that all four structures were also observed in the theoretical results of Jain and Thompson [10] and Machado *et al.* [13], although shifted to higher energies in the latter. In contrast, the calculations of Gianturco [11] and Varella *et al.* [14] (not shown) present no minima in their ICS's or MTCS's. In the previous studies of Gulley *et al.* and of Machado *et al.*, those minima were not assigned as due to the Ramsauer-Townsend effect. The first resonance (at 3 eV) was assigned as a $^2B_2$ shape resonance [10,13] and the second (around 7 eV) was assigned by Jain and Thompson as being of $^2A_1$ symmetry. In order to better understand the physical origin of the structures seen in our calculated results, in Fig. 7(a) we present the eigenphase sums in the (0.5–10)-eV range. From the analysis of this figure, we can conclude that the maximum centered at around 3 eV is indeed due to a $^2B_2$ shape resonance. Further, the significant increase of the eigenphase sums for $^2A_1$ symmetry in the (5–8)-eV region suggests the existence of a possible shape resonance also in this scattering channel. Besides, the minimum seen in the eigenphase sum around 1.5 eV in the $^2A_1$ symmetry indicates the presence of a probable Ramsauer-Townsend mimimum in that energy region. Indeed, these expectations are confirmed, as can be seen in Fig. 7(b), where we plot the individual eigenphases δ_{00} (i.e., corresponding to $l=0,h=0$), δ_{10}, δ_{20}, and δ_{22} of the $^2A_1$ symmetry. It is clearly seen that δ_{00} vanishes at around 1.3 eV and 5.8 eV. This fact can certainly be identified as the origin of the two minima observed in our calculated data. Also, the δ_{00} and δ_{22} waves are responsible for the resonancelike peak seen at around 7 eV, although it is very difficult to associate a shape resonance to an *s*-wave scattering, since no centrifugal barrier is involved in such interactions. From the above analysis, we conclude that the two minima seen both in our calculated ICS's and in the experimental TCS's, located at about 1.5 and 4 eV, respectively, are indeed originated by Ramsauer-Townsend effects. In addition, the resonances seen at around 3 and 7 eV are identified as being of $^2B_2$ and $^2A_1$ symmetries, respectively.

Considering the scarcity of both theoretical and experimental cross sections for elastic electron scattering by this important gaseous molecule, it is hoped that the results reported in the present study can be useful for applications in plasma modeling and atmospheric studies. For the sake of completeness, we present our calculated cross sections in Tables I and II and our measured cross sections in Table III.

[1] S. Trajmar, D. F. Register, and A. Chutjian, Phys. Rep. **97**, 219 (1983).
[2] D. Bockelee-Morvan, P. Colom, J. Crovisier, D. Despois, and G. Paubert, Nature (London) **350**, 318 (1991).
[3] R. J. Gulley, M. J. Brunger, and S. J. Buckmann, J. Phys. B **26**, 2913 (1993).
[4] D. Rolle, H. Kalfa, and H. E. Buhler, Werkst. Korros. **44**, 1 (1993).
[5] R. Tenne, L. Margulis, M. Genut, and G. Hodes, Nature (London) **360**, 444 (1992).
[6] C. Ruset, A. Bloyce, and T. Bell, Surf. Eng. **11**, 308 (1995).
[7] V. F. Sokolov and Y. A. Sokolova, Sov. Tech. Phys. Lett. **7**, 268 (1981).
[8] C. Szmytkowski and K. Maciąg, Chem. Phys. Lett. **129**, 321 (1986).
[9] T. Nishimura and Y. Itikawa, J. Phys. B **29**, 4213 (1996).
[10] A. Jain and D. G. Thompson, J. Phys. B **17**, 443 (1983).
[11] F. A. Gianturco, J. Phys. B **24**, 4627 (1991).
[12] R. Greer and D. G. Thompson, J. Phys. B **27**, 3533 (1994).
[13] L. E. Machado, E. P. Leal, M.-T. Lee, and L. M. Brescansin, J. Mol. Struct.: THEOCHEM **335**, 37 (1995).
[14] M. T. do N. Varella, M. H. F. Bettega, M. A. P. Lima, and L. G. Ferreira, J. Chem. Phys. **111**, 6396 (1999).
[15] A. Zecca, G. P. Karwasz, and R. S. Brusa, Phys. Rev. A **45**, 2777 (1992).
[16] M. V. V. S. Rao and S. K. Srivastava, J. Geophys. Res. [Planets] **98**, 13 137 (1993).
[17] A. Jain and K. L. Baluja, Phys. Rev. A **45**, 202 (1992).
[18] K. N. Joshipura, M. Vinodkumar, and U. M. Patel, J. Phys. B **34**, 509 (2001).
[19] Y. Jiang, J. Sun, and L. Wan, Phys. Rev. A **52**, 398 (1995).
[20] A. K. Jain, A. N. Tripathi, and A. Jain, Phys. Rev. A **42**, 6912 (1990).
[21] D. W. Norcross and L. A. Collins, Adv. At. Mol. Phys. **18**, 341 (1982).
[22] T. N. Rescigno, A. E. Orel, A. U. Hazi, and B. V. McKoy, Phys. Rev. A **26**, 690 (1982).
[23] S. K. Srivastava, A. Chutjian, and S. Trajmar, J. Chem. Phys. **63**, 2659 (1975).
[24] R. T. Brinkman and S. Trajmar, J. Phys. E **14**, 245 (1981).
[25] M. A. Khakoo and S. Trajmar, Phys. Rev. A **34**, 138 (1986).
[26] J. C. Nickel, P. W. Zetner, G. Shen, and S. Trajmar, J. Phys. E **22**, 730 (1989).
[27] M. J. Brunger, S. J. Buckman, D. J. Newman, and D. T. Alle, J. Phys. B **24**, 1435 (1991).
[28] D. T. Alle, R. J. Gulley, S. J. Buckman, and M. J. Brunger, J. Phys. B **25**, 1533 (1992).
[29] S. J. Buckman, R. J. Gulley, M. Moghbelalhossein, and S. J. Bennett, Meas. Sci. Technol. **4**, 1143 (1993).
[30] M. A. Khakoo, T. Jayawera, S. Wang, and S. Trajmar, J. Phys. B **26**, 4845 (1993).
[31] H. Tanaka, T. Ishikawa, T. Masai, T. Sagara, L. Boesten, M. Takekawa, Y. Itikawa, and M. Kimura, Phys. Rev. A **57**, 1798 (1998).
[32] R. R. Lucchese, G. Raseev, and V. McKoy, Phys. Rev. A **25**, 2572 (1982).
[33] A. W. Fliflet and V. McKoy, Phys. Rev. A **21**, 1863 (1980).
[34] M.-T. Lee and V. McKoy, Phys. Rev. A **28**, 697 (1983).
[35] M.-T. Lee, S. Michelin, L. E. Machado, and L. M. Brescansin, J. Phys. B **26**, L203 (1993).
[36] M. E. Rose, *Elementary Theory of Angular Momentum* (John Wiley, New York, 1957).

[37] A. Jain and D. G. Thompson, Comput. Phys. Commun. **30**, 301 (1983).
[38] P. G. Burke, N. Chandra, and F. A. Gianturco, J. Phys. B **5**, 2212 (1972).
[39] S. Huzinaga, Chem. Phys. **42**, 1302 (1965).
[40] I. Cacelli, V. Caravetta, A. Rizzo, and R. Moccia, J. Chem. Phys. **102**, 1230 (1995).
[41] N. T. Padial and D. W. Norcross, Phys. Rev. A **29**, 1742 (1984).
[42] J. O. Hirschfelder, C. F. Curtis, and R. B. Bird, *Molecular Theory of Gases and Liquids* (John Wiley, New York, 1954).
[43] G. Staszewska, D. W. Schwenke, and D. G. Truhlar, Phys. Rev. A **29**, 3078 (1984).
[44] I. Iga, M.-T. Lee, M. G. P. Homem, L. E. Machado, and L. M. Brescansin, Phys. Rev. A **61**, 22708 (2000).
[45] D. R. Olander and V. Kruger, J. Appl. Phys. **41**, 2769 (1970).
[46] A. Roth, *Vacuum Technology* (North-Holland Publishing Co., Amsterdam, 1982).
[47] D. V. Lide (Ed.-in-Chief), *Handbook of Chemistry and Physics*, 73rd ed. (CRC Press, Boca Raton, FL, 1993).
[48] R. H. J. Jansen, F. J. de Heer, H. J. Luyken, B. van Wingerden, and H. J. Blaauw, J. Phys. B **9**, 185 (1976).
[49] B. P. Marinkovič, Ph.D. thesis, University of Beograd, 1985 (unpublished).
[50] J. B. Furness and I. E. McCarthy, J. Phys. B **6**, L42 (1973).
[51] R. Panajotovič, D. Filipovič, B. Marinkovič, V. Pejcev, M. Kurepa, and L. Vuskovič, J. Phys. B **30**, 5877 (1997).
[52] L. E. Machado, L. M. Brescansin, and M.-T. Lee, Braz. J. Phys. **32**, 804 (2002).